Chinese Chemical Letters 32 (2021) 2317–2321

Contents lists available at ScienceDirect

Chinese Chemical Letters

journal homepage: www.elsevier.com/locate/cclet

Communication

Built-in piezoelectric field improved photocatalytic performance of nanoflower-like Bi_2WO_6 using low-power white LEDs

Hua Lei, Meixuan Wu, Ying Liu, Fan Mo, Jiayao Chen, Shilong Ji, Yan Zou, Xiaoping Dong*

Department of Chemistry, Key Laboratory of Surface & Interface Science of Polymer Materials of Zhejiang Province, Zhejiang Sci-Tech University, Xiasha Higher Education Zone, Hangzhou 310018, China

ARTICLE INFO

Article history:
Received 25 September 2020
Received in revised form 16 November 2020
Accepted 10 December 2020
Available online 16 December 2020

Keywords:
Photopiezocatalysis
LED illumination
Ultrasonic vibration
Piezoelectric effect
Dye degradation

ABSTRACT

Photocatalysis technology has been proved to be a potential strategy for removal of organic dyes, however high-power light sources are generally necessary to initiate photocatalytic reaction. In this work, we employed an excellent photocatalyst of Bi_2WO_6 with visible light harvest and meanwhile an intrinsic ferroelectricity, which realized the efficient degradation of organic dye *via* the synergetic photopiezocatalysis. Through coupling the illumination by a low-power (9 W) LED and the ultrasonic vibration (120 W) by an ultrasonic cleaner, the nanoflower-like Bi_2WO_6 composed of ultrathin nanosheets showed a much more enhanced photopiezocatalysis performance for purification of organic dye than the individual photocatalysis and piezocatalysis. Furthermore, the high mineralization efficiency and the good durability of the Bi_2WO_6 catalyst were demonstrated. The possible mechanism of photopiezocatalysis was finally proposed, where the ultrasound-induced piezoelectric field in Bi_2WO_6 drove photo-generated electrons and holes to diffuse along opposite directions, consequently promoting the separation efficiency of charge carriers. This work indicates that the synergetic photopiezocatalysis by coupling irradiation and ultrasonic vibration is a promising strategy to purify organic pollutants in wastewater.

Semiconductor photocatalysis technology has attracted extensive research interests because it is an environmentally friendly and energy-saving process for converting photo-energy to chemical energy [1–3]. Nevertheless, due to the insufficient utilization of sunlight and the low quantum efficiency of photoconversion, the photocatalytic activity of current photocatalysts is not satisfactory enough to guarantee its practical applications [4,5]. Especially, photocatalysis investigation in the laboratory is usually initiated by a high-power light source with a high percentage of UV light, such as mercury lamp and xenon lamp, which is absent in nature light or indoor illumination. Consequently, it is highly desirable to develop new strategies to achieve high photocatalytic activity under low-power light source irradiation.

Very recently, a new concept of piezocatalysis has been proposed based on the piezoelectric effect, which realizes the conversion from mechanical energy to chemical energy [6–8]. In principle, the strain-induced piezoelectric polarization will result in the accumulation of bound positive and negative charges on opposite surfaces of the piezoelectric crystal. To balance these bound charges, some opposite charges will be adsorbed on the surface, and therefore be involved in surface redox reaction driven by the piezoelectric potential [9–11]. On the other hand, some researchers consider that the piezocatalysis originates from the phonon-excited free charges that are accumulated on opposite surfaces of piezoelectric semiconductor from the oriented migration with the built-in piezoelectric field [12–14].

It has been demonstrated that coupling light excitation and piezoelectric polarization is an effective pathway to greatly enhance the catalytic performance [15–17]. In general, there are two methods to realize this coupling in catalyst systems (Fig. S1 in Supporting information). One is combination of a photocatalyst with a piezoelectric material, the polarized piezoelectric material acts as an external piezoelectric field, whose bound charges on the interface will attract photo-excited carriers with opposite charge and simultaneously exclude those bearing same charge, consequently promoting the separation of photo-generated electrons (e^-) and holes (h^+) in photocatalyst [18,19]. The other is use of a semiconductor material that simultaneously possesses piezoelectric and photo-response properties. The formed built-in piezoelectric field can drive the internal photo-produced e^- and h^+ to migrate to opposite surfaces [20,21]. In comparison with the composite, the piezoelectric photocatalyst provides more surface

* Corresponding author.
E-mail address: xpdong@zstu.edu.cn (X. Dong).

https://doi.org/10.1016/j.cclet.2020.12.019
1001-8417/

loaded charge carriers for a redox reaction to produce reactive oxygen species (ROS, *e.g.*, photo-induced hole, hydroxyl radical and superoxide radical) [22–25].

As one of the simplest members of Aurivillius oxides, Bi_2WO_6 has a layered structure with alternating bismuth oxide $(Bi_2O_2)^{2+}$ and octahedral $(WO_4)^{2-}$ sheets (Fig. 1A), which is favorable for charge transfer. Besides the promising photocatalytic behavior, Bi_2WO_6 simultaneously possesses unique physical properties such as ferroelectricity associated with large spontaneous polarization [26–28]. In this work, we revealed the synergetic enhancement of Bi_2WO_6 photopiezocatalysis through the coupling of visible-light irradiation and ultrasonic vibration. A 120 W ultrasonic cleaner was used to provide the external mechanical force to the vibration of the Bi_2WO_6 sample, and a low-power white LED (9 W) was employed as a light source to generate free charge carriers. Driven by the internal piezoelectric field, these photo-excited e^- and h^+ migrated along opposite directions, resulting in greatly suppressing the recombination of these e^- and h^+. The synergetic photopiezocatalysis of Bi_2WO_6 showed significantly increased activity for the removal of organic dye in comparison with the single photocatalysis and piezocatalysis. We also studied the stability and durability of the catalyst, and finally proposed a possible mechanism of the photopiezocatalysis to explain the activity improvement of Bi_2WO_6.

The crystal phase of Bi_2WO_6 was analyzed by the X-ray diffraction (XRD) technology (Fig. 1B). The diffraction peaks of Bi_2WO_6 could be indexed to the orthorhombic Bi_2WO_6 phase (PDF# 73–2020). No peaks belonging to other phases are observed, indicating the high purity of the catalyst. The optical property of the as-prepared Bi_2WO_6 catalyst was measured by UV–vis diffuse reflectance spectroscopy (DRS). The Bi_2WO_6 exhibits an intensive absorption onset located at ~450 nm (Fig S2A in Supporting information), implying the possibility of utilizing sunlight on this catalyst to drive the photocatalytic reaction. Meanwhile, its band gap (E_g) value was calculated to be ~2.64 eV (Fig. S2B in Supporting information). The morphologic features of the catalyst were characterized by scanning electron microscope (SEM) and transmission electron microscope (TEM). SEM image of Bi_2WO_6 (Fig. 1C) shows that most sample particles present spherical shapes, and their particle size is about 3 μm (Fig. 1D). The Bi_2WO_6 particle is composed of numerous 2D nanosheets that vertically align on the particle surface, just like a "nanoflower" where these nanosheets act as petals. The thickness of Bi_2WO_6 nanosheets is further determined as 10~20 nm, meanwhile possessing a large lateral size of several hundred nanometers (Fig. 1E). This typical 2D structure with large aspect ratio is expected to be easily bended as an external mechanical force is performed, like the reported 1D and 2D nanostructure piezocatalysts or photopiezocatalysts [8,10,11,29]. Fig. 1F depicts a single Bi_2WO_6 particle that has similar diameter to the SEM result and possesses lots of flash burrs on the surface. These flash burrs are further determined to 2D Bi_2WO_6 nanosheets from the high-magnification TEM image (Fig. 1G). Fig. 1H illustrates the high-resolution TEM (HRTEM) image of the Bi_2WO_6 catalyst. Two mutually perpendicular sets of clear fringes are observed. The calculated *d* spacing values are 0.274 nm and 0.273 nm, respectively corresponding to the (200) and (020) planes of the orthorhombic Bi_2WO_6 (inset of Fig. 1H).PDF

The photopiezocatalytic performance of Bi_2WO_6 was estimated through degradation of rhodamine B (RhB) under simultaneous illumination by a 9 W white LED and vibration by 120 W ultrasonic cleaner. Fig. 2A compares the RhB degradation efficiencies under different catalytic modes, and the related absorption spectra of RhB are shown in Fig. S3 (Supporting information). With the absence of the catalyst, a slight decrease of RhB concentration was taken place under ultrasound treatment for 60 min, which can be ascribed to the activation of water initiated by ultrasound [30]. In the

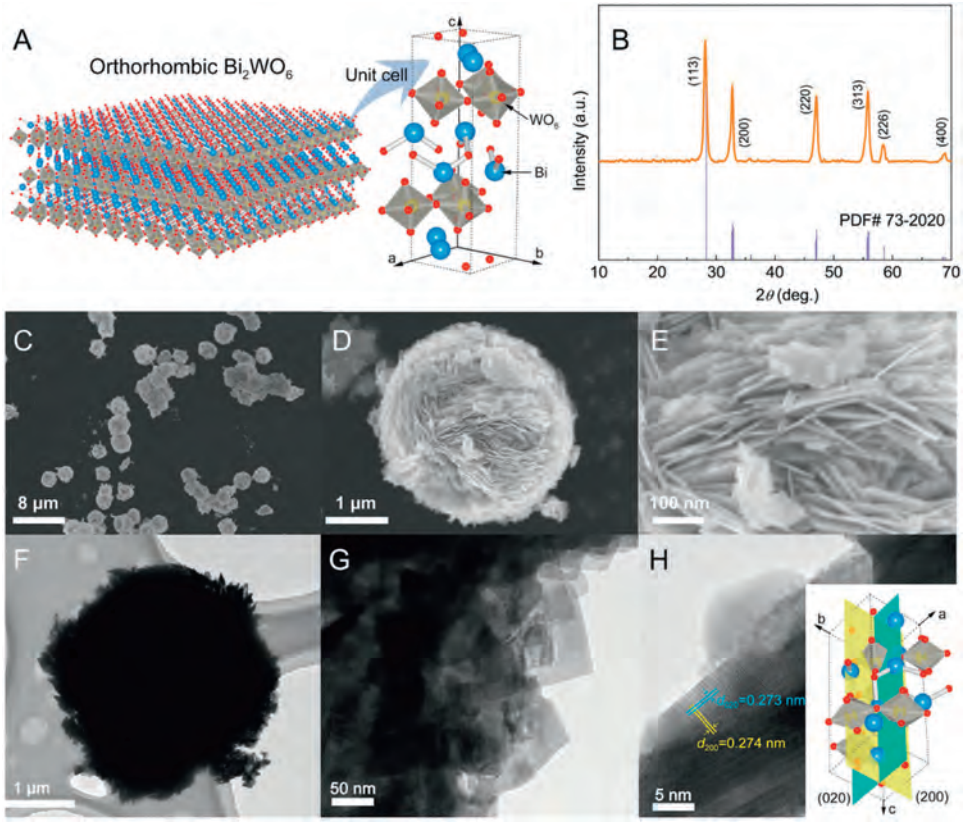

Fig. 1. Structural characterizations of Bi_2WO_6: (A) Crystallographic structure model, (B) XRD pattern, (C, D, E) SEM, (F, G) TEM and (H) HRTEM images.

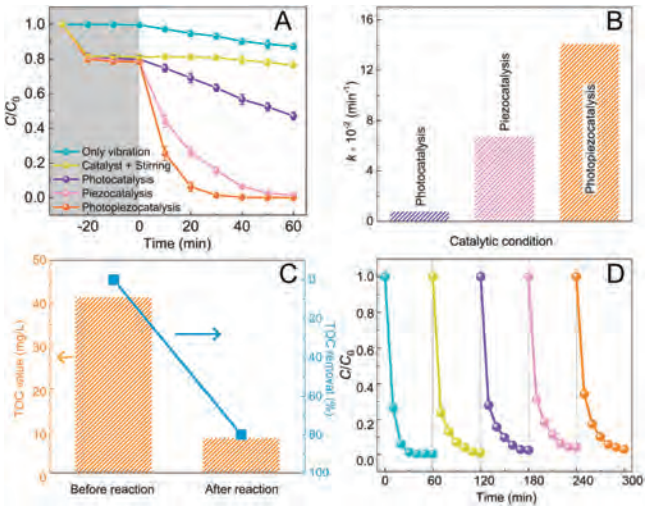

Fig. 2. (A) Catalytic efficiencies, (B) *pseudo*-first order kinetics of RhB degradation by Bi_2WO_6 under various catalytic conditions. (C) TOC changes of RhB solution. (D) Cycling stability of Bi_2WO_6 for photopiezocatalysis of RhB.

meantime, no RhB except for the surface adsorption effect was removed by the Bi_2WO_6 catalyst without vibration treatment. After 60 min of treatment, the RhB removal ratio is 49% for photocatalysis and 100% for piezocatalysis. The synergetic photopiezocatalysis has a much higher activity, where > 70% RhB was removed in the first 10 min, and a complete removal was achieved after 30 min simultaneous illumination/vibration treatment. The apparent rate constant (k) was calculated as the slope of the $\ln(C/C_0)$ against time (t) plot, on the basis of the pseudo-first-order kinetics. The terms C and C_0 are the instantaneous and initial concentrations of RhB at 554 nm, respectively. The observed k value (Fig. 2B) of photopiezocatalysis is 0.141 min^{-1}, which is 17.5 and 2.1 times of those from photocatalysis and piezocatalysis, respectively. To reveal the mineralization of RhB, the TOC values of RhB concentration before and after photopiezocatalysis were measured (Fig. 2C). It can be seen that the TOC value drops from the initial 41.4 mg/L to 8.39 mg/L, obtaining an effective TOC removal rate of about 79.7%. This result indicates that most RhB molecules were completely degraded to CO_2 and H_2O. Considering the reusability and stability of the catalyst are important for practical application, five successive degradation tests were conducted. A similar level of activity (Fig. 2D) is maintained after five cycles, suggesting the high stability and reusability of the Bi_2WO_6 catalyst under ultrasonic vibration and light irradiation. Moreover, the XRD patterns before and after photopiezocatlaysis confirm the crystal structure of Bi_2WO_6 is remained (Fig. S4 in Supporting information). SEM images of the used Bi_2WO_6 (Fig. S5 in Supporting information) show no significant size change (~3 μm) compared with the fresh Bi_2WO_6 in Fig. 1D, but the microsphere structure slightly collapsed after violent ultrasound treatment.

The synergetic photopiezocatalysis mechanism of Bi_2WO_6 is discussed in Fig. 3. The Bi_2WO_6 has a relatively small E_g value and then can harvest a portion of visible light to excite e^- from the valence band (VB) to the conduction band (CB), therefore leaving h^+ on VB (Fig. 3A). Though the Bi_2WO_6 has a built-in electric field (E_1) due to the intrinsic ferroelectricity, opposite charges will be adsorbed from solution onto the surface to balance the bound charges. These adsorbed charges will provide an external electric field (E_2) that is equivalent but antiparallel to the built-in electric field. Thus, the inner net electric field of Bi_2WO_6 is zero, which results in most of these photo-generated e^- and h^+ attempt to recombine before diffusing to the catalyst surface. This low photoquantum efficiency combined with the low power of the white LED lamp induces the weak photocatalytic performance of Bi_2WO_6. In the piezocatalysis mode, the ultrasound-induced strain causes the intensity change of Bi_2WO_6 polarization. Fig. 3B gives an example of the polarization increase, in which the built-in piezoelectric field in Bi_2WO_6 (E_1) is larger than the external electric field (E_2). Driven by the built-in piezoelectric field, the excited free e^- and h^+ are efficiently separated, but the concentration of the phonon-excited free charge carriers is quite low. When coupling these two catalytic modes, the photo-generated e^- and h^+ in Bi_2WO_6 will diffuse towards opposite directions, therefore promoting the separation of charge carriers (Fig. 3C), which was further demonstrated by testing the current responses under different catalytic modes

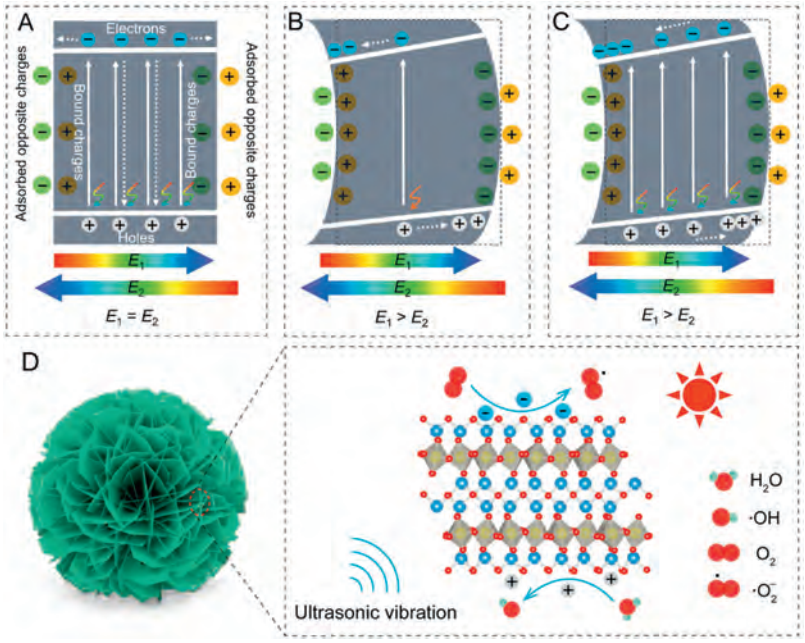

Fig. 3. Band diagrams of Bi_2WO_6 at various catalytic modes: (A) Photocatalysis, (B) piezocatalysis and (C) photopiezocatalysis. (D) Schematic illustration for the photopiezocatalysis of Bi_2WO_6 under the visible light irradiation/ultrasonic vibration treatments.

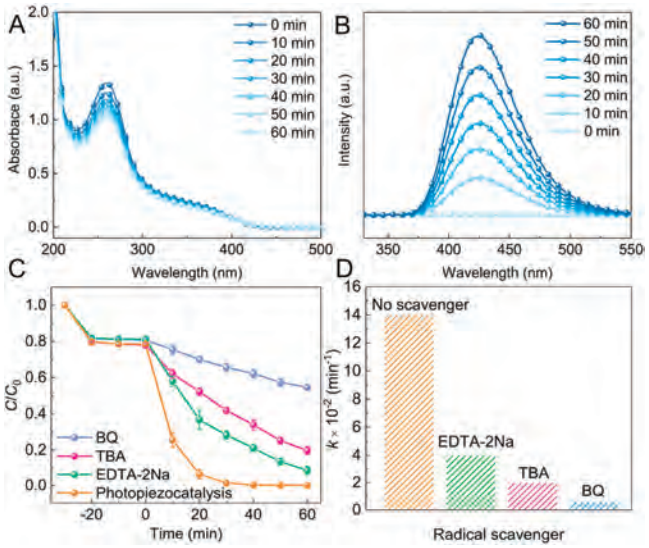

Fig. 4. (A) UV–vis absorption spectra of the NBT solution and (B) fluorescence spectra of the terephthalic acid solution with the presence of Bi_2WO_6 under the visible light irradiation/ultrasonic vibration treatments. (C) Photopiezocatalytic decomposition of RhB with Bi_2WO_6 in the presence of different radical scavengers. (D) The observed kinetic rate constant after adding different radical scavengers.

(Fig. S6 in Supporting information). It is obviously found that the synergetic irradiation/ultrasonic treatment exhibited a much higher current response than those under the single irradiation and ultrasound conditions. Based on the above discussion, the feasibly photopiezocatalytic mechanism of Bi_2WO_6 for removing RhB is schematically presented in Fig. 3D. Bi_2WO_6 is a piezoelectric semiconductor and its piezoelectricity originates from the coherent deviation of W atoms in WO_6 octahedron parallel to the planer surface [31]. The nanoflower-like Bi_2WO_6 sample is composed of numerous 2D nanosheets that easily produce strains by the so-called "cavitation phenomenon" in the ultrasonic treatment [32]. The strain-induced polarization change provides an electric field force to drive photo-generated e^- and h^+ to transfer towards opposite surfaces of Bi_2WO_6, greatly suppressing the bulk recombination of charge carriers. These free charges accumulated on different surfaces have strongly redox ability to produce various reactive oxygen species (ROS), such as superoxide radicals ($^{\bullet}O_2^-$) from the reduction reaction of adsorbed O_2 molecules by the photo-generated e^- on CB, and hydroxyl radicals ($^{\bullet}OH$) formed *via* oxidizing water by the photo-produced h^+ on VB. These ROS as well as the photo-excited h^+ have been widely reported to efficiently oxidize organic dye molecules to small molecules (*e.g.*, water and CO_2) [33,34].

To corroborate the photopiezocatalytic mechanism of Bi_2WO_6 for catalytic purification of organic dye, the production of ROS ($^{\bullet}O_2^-$ and $^{\bullet}OH$) was experimentally monitored. We employed the nitro blue tetrazolium (NBT, 0.098 mmol/L) method [35] to illustrate the generation of $^{\bullet}O_2^-$ radicals, which is demonstrated by the gradual decrease of NBT characteristic absorption in the UV–vis spectrum as prolonging the irradiation/ultrasonic vibration treating time (Fig. 4A). It is well known that terephthalic acid (TA) can trap $^{\bullet}OH$ radicals to form 2-hydroxyterephthalic acid (TAOH) that has a unique fluorescence response centered at 425 nm [23]. As shown in Fig. 4B, with an excitation wavelength of 315 nm, the fluorescence intensity increases significantly, indicating the efficient formation of $^{\bullet}OH$ radicals. Electron paramagnetic resonance (EPR) analysis was also applied to identify the ROS (*i.e.*, $^{\bullet}OH$, $^{\bullet}O_2^-$) by using 5,5-dimethyl-1-pyrroline N-oxide (DMPO) as spin-trapping agent. The peak signals of DMPO-$^{\bullet}OH$ (peak intensity ratio of 1:2:2:1) and DMPO-$^{\bullet}O_2^-$ (peak intensity ratio of 1:1:1:1) spin adducts were observed in the photopiezocatalysis of Bi_2WO_6 (Fig. S7 in Supporting information). The essential roles of the reactive species in the photopiezocatalytic degradation were further explored by trapping experiments using benzoquinone (BQ, 0.5 mmol/L), tert-butyl alcohol (TBA, 6 mmol/L), and disodium ethylenediaminetetraacetate (EDTA-2Na, 6 mmol/L), as scavengers for $^{\bullet}O_2^-$, $^{\bullet}OH$ and holes, respectively [36]. It is obvious in Fig. 4C that the distinct inhibitions were observed for the degradation of RhB when the scavengers were introduced into the reaction system. And, the suppressing effect for RhB degradation follows the order: BQ > TBA > EDTA-2Na (Fig. 4D), which was further demonstrated by quantitatively analyzing the production of $^{\bullet}O_2^-$ and $^{\bullet}OH$ radicals (Fig. S8 in Supporting information). These findings further confirm that ROS plays a crucial role in photopiezocatalytic reaction process, suggesting these three active oxidants are responsible for the removal of the dye molecules.

In summary, a high-performance catalytic activity of Bi_2WO_6 was realized through utilizing the synergetic photopiezocatalysis *via* coupling the low-power white LED (9 W) irradiation and the ultrasonic vibration (120 W). The ultrasound-induced build-in piezoelectric field originating from piezoelectric polarization could efficiently suppress the recombination of photo-excited e^- and h^+. The photopiezocatalysis of Bi_2WO_6 realized the efficient degradation of RhB dye, which reaction rate was 17.5 and 2.1 times of those from photocatalysis and piezocatalysis, respectively. And the Bi_2WO_6 exhibited long-term stability and reusability, maintaining its photopiezocatalytic activity at 99% after recycling five runs. We believe that this photopiezocatalysis approach provides a possible strategy for environmental remediation and other catalytic applications by harnessing low-power indoor illumination and the surrounding mechanical energy.

Declaration of competing interest

The authors declare that they have no known competing financial interests or personal relationships that could have appeared to influence the work reported in this paper.

Acknowledgments

This work was financially supported from the National Key Research and Development Program of China (No. 2017YFE0127400) and the Zhejiang Provincial Natural Science Foundation of China (No. LY17B010004).

References

[1] A. Naldoni, M. Altomare, G. Zoppellaro, et al., ACS Catal. 9 (2019) 345–364.
[2] C. Yao, R. Wang, Z. Wang, et al., J. Mater. Chem. A 7 (2019) 27547–27559.
[3] H. Zhang, J. He, C. Zhai, M. Zhu, Chin. Chem. Lett. 30 (2019) 2338–2342.
[4] F. Chen, H. Huang, L. Guo, Y. Zhang, T. Ma, Angew. Chem. Int. Ed. 58 (2019) 10061–10073.
[5] M. Zhang, J. He, Y. Chen, et al., Chin. Chem. Lett. 31 (2020) 2721–2724.
[6] W. Wu, L. Wang, Y. Li, et al., Nature 514 (2014) 470–474.
[7] S. Li, Z. Zhao, J. Zhao, et al., ACS Appl. Nano Mater. 3 (2020) 1063–1079.
[8] X. Xue, W. Zang, P. Deng, et al., Nano Energy 13 (2015) 414–422.
[9] H. You, Z. Wu, L. Zhang, et al., Angew. Chem. Int. Ed. 58 (2019) 11779–11784.
[10] Y. Zhao, X. Huang, F. Gao, et al., Nanoscale 11 (2019) 9085–9090.
[11] X. Xu, Y. Jia, L. Xiao, Z. Wu, Chemosphere 193 (2018) 1143–1148.
[12] J. Wu, N. Qin, D. Bao, Nano Energy 45 (2018) 44–51.
[13] J. Wu, Q. Xu, E. Lin, et al., ACS Appl. Mater. Interfaces 10 (2018) 17842–17849.
[14] E. Lin, J. Wu, N. Qin, et al., Catal. Sci. Technol. 9 (2019) 6863–6874.
[15] M. Wang, Y. Zuo, J. Wang, et al., Adv. Energy Mater. 9 (2019) 1901801.
[16] M. Ismail, Z. Wu, L. Zhang, et al., Chemosphere 228 (2019) 212–218.
[17] Z. Zhao, L. Wei, S. Li, et al., J. Mater. Chem. A 8 (2020) 16238–16245.
[18] C. Sun, Y. Fu, Q. Wang, L. Xing, B. Liu, X. Xue, RSC Adv. 6 (2016) 87446–87453.
[19] W. Tong, Y. Zhang, H. Huang, et al., Nano Energy 53 (2018) 513–523.
[20] Y. Feng, H. Li, L. Ling, et al., Environ. Sci. Technol. 52 (2018) 7842–7848.
[21] J. Zhang, X. Chen, Y. Bai, et al., J. Mater. Chem. A 7 (2019) 10264–10272.
[22] Y. Cui, J. Briscoe, S. Dunn, Chem. Mater. 25 (2013) 4215–4223.
[23] X. Xu, Y. Jia, L. Xiao, Z. Wu, Chemosphere 193 (2017) 1143.

[24] H. You, Y. Jia, Z. Wu, M. Ismail, et al., Electrochem. commun. 79 (2017) 55–58.
[25] S. Lan, Y. Chen, L. Zeng, et al., J. Hazard. Mater. 393 (2020) 122448.
[26] H. Djani, P. Hermet, P. Ghosez, J. Phys. Chem. C 118 (2014) 13514–13524.
[27] A. Hao, X. Ning, Y. Cao, J. Xie, D. Jia, Mater. Chem. Front. 4 (2020) 2096–2102.
[28] Z. Kang, N. Qin, E. Lin, et al., J. Clean. Prod. 261 (2020) 121125.
[29] M. Zelisko, Y. Hanlumyuang, S. Yang, et al., Nat. Commun. 5 (2014) 4284.
[30] A. Hassani, A. Khataee, S. Karaca, C. Karaca, P. Gholami, Ultrason. Sonochem. 35 (2017) 251–262.
[31] H. Djani, E. Bousquet, A. Kellou, P. Ghosez, Phys. Rev. B 86 (2012) 054107.
[32] N.S.M. Yusof, B. Babgi, Y. Alghamdi, et al., Ultrason. Sonochem. 29 (2016) 568–576.
[33] L. Xu, X. Wang, M. Xu, et al., Ultrason. Sonochem. 61 (2020) 104815.
[34] Q. Chen, L. Chen, J. Qi, et al., Chin. Chem. Lett. 30 (2019) 1214–1218.
[35] Y. Li, Y. Zheng, D. Zhang, et al., Chin. Chem. Lett. 28 (2017) 184–188.
[36] H. Lei, H. Zhang, Y. Zou, et al., J. Alloys Compd. 809 (2019) 151840.